

Effect of 1070 nm laser intensity on parameters of In_{0.3}Ga_{0.7}As solar cell

Guangji Li (李广济)¹, Hongchao Zhang (张宏超)^{1,**}, Chengmin Wang (王程民)^{1,2}, Yunxiang Pan (潘云香)¹, Jian Lu (陆健)^{1,*}, and Dayong Zhou (周大勇)³

¹School of Science, Nanjing University of Science and Technology, Nanjing 210094, China

²College of Mechanical Engineering, Huaian Vocational College of Information Technology, Huaian 223003, China

³State Key Laboratory of High-Efficiency Power Conversion, Shanghai Institute of Space Power-Sources, Shanghai 200245, China

*Corresponding author: lujian@mail.njust.edu.cn; **corresponding author: hongchao@njust.edu.cn

Received September 29, 2018; accepted December 7, 2018; posted online February 27, 2019

The photoelectric properties of In_{0.3}Ga_{0.7}As solar cells applied in laser wireless power transmission (LWPT) were studied when they were irradiated by 1070 nm continuous wave (CW) laser of various intensities. The influences of laser intensity on solar cell parameters extracted by the pollination algorithm were analyzed quantitatively. Results show that the conversion efficiency of the cell rose to the maximum and then decreased rapidly in the laser intensity range of 50–900 mW/cm². With higher energy laser irradiation, the rise of ideality factor and reverse saturation current would lead to the degradation of voltage at the maximum power point, which was the main reason for the decrease of conversion efficiency. The results provide the basis for choosing the appropriate input energy in the case of different transmission systems.

OCIS codes: 160.6000, 260.2160.

doi: 10.3788/COL201917.031601.

Laser wireless power transmission (LWPT) was first proposed by Glaser^[1] in 1968, who attempted to transmit the solar energy outside the atmosphere to the ground by laser and then converted it into electricity by solar cells. Compared with other wireless energy transmissions, LWPT owns the advantages of long transmission distance, high energy density, and dynamic transmission. Therefore, it can be widely applied in spacecraft, space bases, drones, robots, and fast charging^[2–4].

A solar cell is the determinant factor of laser–electrical conversion efficiency at the receiving end of LWPT^[5–8], as well as one of the main factors limiting the development of LWPT systems. Wireless power transmission of high energy density can be achieved by laser, in which high laser energy irradiates on small-area solar cells. Therefore, study on the photoelectric properties of solar cells under high laser illumination is very important for evaluating cell performance and selecting appropriate input laser energy for LWPT systems in different situations^[9].

Generally, the photoelectric properties of a solar cell could be characterized by several parameters, such as the short circuit current (I_{sc}), open circuit voltage (V_{oc}), fill factor (FF), and efficiency (η)^[10]. The efficiency of the solar cell depends on the I_{sc} , V_{oc} , FF, and light intensity (P_{laser}) and can be expressed as

$$\eta = \frac{I_{sc} \cdot V_{oc} \cdot FF}{P_{laser}}, \quad (1)$$

$$FF = \frac{I_m \cdot V_m}{I_{sc} \cdot V_{oc}}, \quad (2)$$

where I_m and V_m represent the current and voltage at the maximum power point, respectively.

The current–voltage (I – V) characteristics provide the most important information of the performance of the solar cell, which is usually described based on one diode model as

$$I = I_{ph} - I_0 \left\{ \exp \left[\frac{q(V - IR_s)}{nkT} \right] - 1 \right\} - \frac{V - IR_s}{R_{sh}}. \quad (3)$$

In Eq. (3), I_{ph} is the photo-generated current, n is the diode ideality factor, I_0 is the reverse saturation current, R_{sh} and R_s are the series and parallel resistance, respectively, q is the electron charge, k is the Boltzmann constant, and T is the temperature of the cell.

The parameters mentioned above control the I – V characteristics of a cell at any given intensity of illumination and thus decide the values of the performance parameters and the efficiency of the cell. n and I_0 both provide information about the charge recombination in the bulk space charge regions and the surface of the cell. FF is strongly affected by n and I_0 . Moreover, V_{oc} basically depends on R_{sh} , n , and I_0 and is inversely proportional to I_0 . As it is depicted in Ref. [11], a higher n would introduce a higher V_{oc} but a lower FF. Therefore, accurate extraction of solar cell parameters under laser irradiation is of great importance for applications of LWPT.

Several methods have been proposed to extract parameters of the cell using I – V characteristics^[12–19], in which the pollination algorithm was adopted, widely due to its advantages of simple operation, convenient implementation, and strong optimization ability. It is a global convergence

search algorithm proposed by Yang in 2012 inspired by the pollination process^[20]. Compared with other algorithms for extracting solar cell parameters, the pollination algorithm has higher convergence speed and parameter precision and is suitable for extracting parameters under different temperature and illumination conditions^[17]. Due to the advantages above, the pollination algorithm was selected to extract the parameters of solar cells with the single-diode model in our research.

A fiber laser has higher photoelectric conversion efficiency and beam quality. It has wavelengths near 1000 nm, which are in the atmospheric window, and there is less transmission loss in the atmosphere. With the development of fiber lasers, the output power is increasing^[21,22]. So, it is suitable for the LWPT system using fiber laser to transmit with longer distance and higher energy density^[23]. As depicted above, a continuous fiber laser with the wavelength of 1070 nm was selected to irradiate $\text{In}_{0.3}\text{Ga}_{0.7}\text{As}$ solar cells to investigate the dependence of laser intensity and performance of solar cells. Various laser power densities ranging from 50 to 900 mW/cm^2 were incident to the surface of solar cells in our experiments.

The solar cell used in this experiment was a single-junction $\text{In}_{0.3}\text{Ga}_{0.7}\text{As}$ solar cell fabricated by metal organic chemical vapor deposition (MOCVD) technology by the Shanghai Institute of Space Power-Sources^[24]. The schematic diagram of the solar cell is shown in Fig. 1(a). The front surface was $1\text{ cm} \times 1\text{ cm}$, as shown in Fig. 1(b), and the emitter region was n-doped, forming an np-type structure. The energy gap of $\text{In}_{0.3}\text{Ga}_{0.7}\text{As}$ material was $E_g = 1.01\text{ eV}$. The temperature of the back surface of the solar cell was controlled at $25 \pm 1^\circ\text{C}$ by a thermostat. A digital source meter was used to test and record the I - V curves of the cell at different laser irradiation levels.

The vector solution defined as $(R_s, R_{sh}, I_s, n, I_{ph})$ can be derived by the pollination algorithm within the ranges as follows^[17,25]:

$$\begin{aligned} R_s &\in [0, 2\ \Omega], \\ R_{sh} &\in [0, 5000\ \Omega], \\ I_s &\in [0, 1\ \mu\text{A}], \\ n &\in [1, 5], \\ I_{ph} &\in [0, 2I_{sc}]. \end{aligned} \quad (4)$$

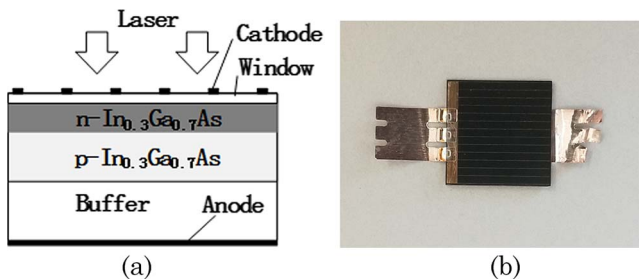


Fig. 1. (a) Schematic diagram of $\text{In}_{0.3}\text{Ga}_{0.7}\text{As}$ solar cell. (b) The picture of the solar cell.

The objective function of the optimization algorithm was the root mean square error (RMSE). Finally, the five parameters obtained by the algorithm were used to calculate the I - V curves by the Newton method.

Ten groups of I - V curves of the solar cell with different laser energies were obtained. In the process of extracting five parameters, the calculated objective function RMSE was less than 3.87×10^{-4} . The I - V curves are shown in Fig. 2, in which the solid symbols are the experimental results, and the lines denote the results calculated by the five parameters. The unit of incident laser intensity (P_{laser}) is milliwatts per centimeter squared (mW/cm^2).

As can be seen from Fig. 2, the calculation results are consistent with the experimental results, and there is no significant difference between the two. This proves that it is reasonable to use the single-diode model to study the output characteristics of solar cells under laser irradiation and also verifies the high precision of the pollination algorithm in solving the five parameters of solar cells.

The performance parameters and the maximum power point of the solar cell can be easily extracted from Fig. 2 as well. The relationships between I_{sc} and I_m with laser power are shown as Fig. 3. With the increase of P_{laser} , I_{sc} increases linearly. The blue hollow squares in the figure are experimental results, and the blue line is the linear fitting result with a fitting function of

$$I_{sc} = 5.1 \times 10^{-4} P_{\text{laser}} + 0.0014. \quad (5)$$

It could be clearly observed that the curve did not pass through the origin, because the experiment was carried out in a non-dark room environment, in which the scattered light from the ambient environment induced photo-generated carriers inside the cell. The red solid squares in the figure are I_m . Likewise, I_m was nearly proportional to P_{laser} with a smaller slope than that of I_{sc} .

Figure 4 shows the variation of V_{oc} and V_m with P_{laser} . The V_{oc} value (blue solid squares) increased exponentially with increasing P_{laser} , and the value increased by 14.3% in the range of 50–900 mW/cm^2 . The V_m value (red hollow

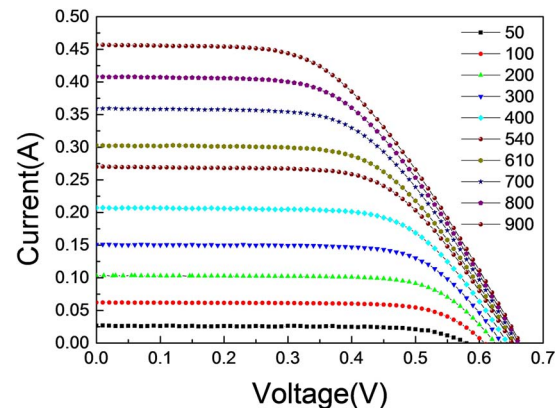


Fig. 2. I - V curves of the solar cell under different laser power densities. (The dots are experimental results, and the lines are calculation results. The unit of P_{laser} is mW/cm^2 .)

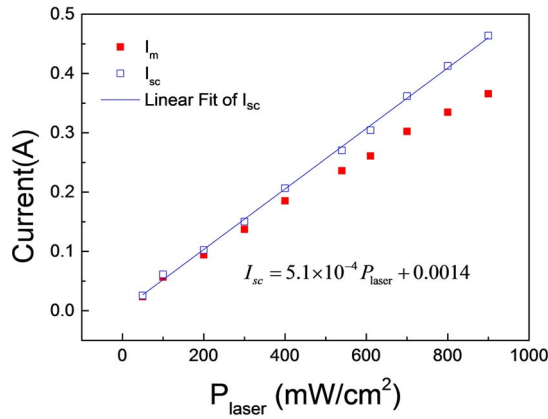


Fig. 3. Effects of P_{laser} on the current at short circuit and maximum power point. (The function in the figure is a linear fitting function of the short circuit current.)

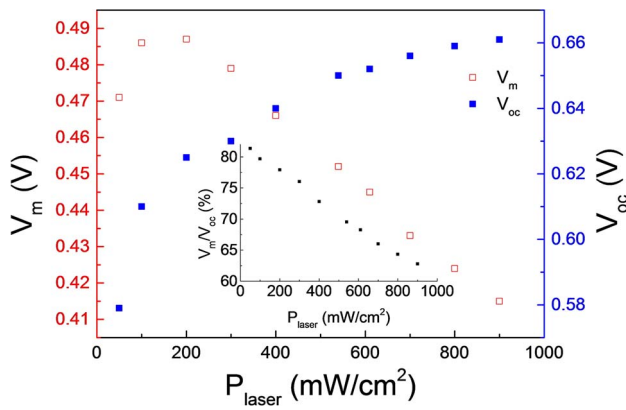


Fig. 4. Effects of P_{laser} on the voltage at open circuit and maximum power point. The inset shows the relationship between V_{oc}/V_m and P_{laser} .

squares) increased to the maximum value of about 0.49 V between 100 and 200 mW/cm^2 and then began to decrease linearly with a further increase of P_{laser} . The inset shows the dependence of V_{oc}/V_m values on P_{laser} . The ratio of V_{oc}/V_m dropped linearly from 82% at 50 mW/cm^2 to 62% at 900 mW/cm^2 . It could be concluded that when the V_{oc} value rose, the V_m value decreased, and the descending speed was higher than that of the increasing speed. With the increase of the P_{laser} value, V_m of the solar cell decayed rapidly. The results of I_{sc} and V_{oc} induced by laser irradiation were similar to those irradiated by sunlight^[26].

Figure 5 illustrates the dependency of the FF and η values on P_{laser} . The FF value (red solid squares in the graph) increased slightly to the maximum of 0.755 near 100 mW/cm^2 and then dropped linearly to 0.495 at 900 mW/cm^2 . The relationship between η and P_{laser} is similar to that of FF and P_{laser} , and the maximum value of η was about 27.5% near 100 mW/cm^2 and then decreased rapidly to 16.8%.

According to Eqs. (1) and (2), FF and η were directly related to I_m and V_m . I_m increased linearly with P_{laser} ,

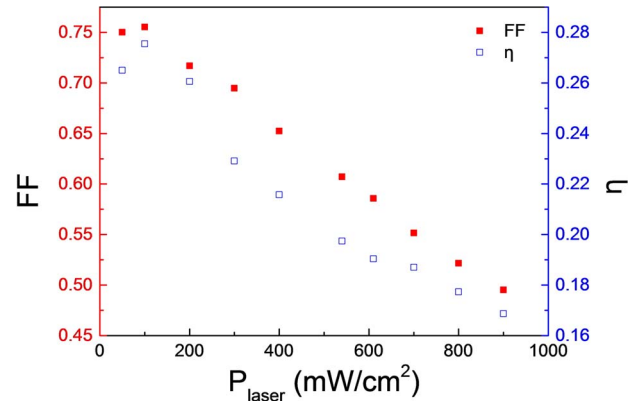


Fig. 5. Effects of P_{laser} on fill factor and conversion efficiency.

while the value of V_m increased at first and then decreased with the increase of P_{laser} . The evolution trends of V_m , FF, and η were similar. Therefore, the main cause of the decrease in FF and η could be attributed to the attenuation of V_m . The relationship between η and P_{laser} obtained in our experiments is the same as that in Ref. [9], in which the light-to-electricity conversion efficiency decreases with increased input laser power density (with $P_{\text{laser}} > 100 \text{ mW}/\text{cm}^2$) invariably. In order to find out the genesis of the behaviors of solar cells to laser irradiation, the dependences of the five parameters on P_{laser} were investigated in the next paragraphs.

Figure 6 depicts the dependences of the R_s and R_{sh} values on P_{laser} . As the value of P_{laser} increased, R_s and R_{sh} decreased similarly, and the rate of decline became smaller. In the range of 50–900 mW/cm^2 , the relative changes of R_s and R_{sh} were 41.2% and 52.3%, respectively. According to Ref. [26], current leakage represented by R_{sh} would occur at the edge with local defects of the solar cell. Defects increase the concentration of local traps, forming active regions of recombination, which would capture photo-generated minority carriers^[26,27]. With further increase of P_{laser} , solar cell performance degradation was also reflected in the decrease in R_{sh} ^[11], which was one of the reasons leading to the decrease of V_m as well. Series resistance comes from electrode contact resistance

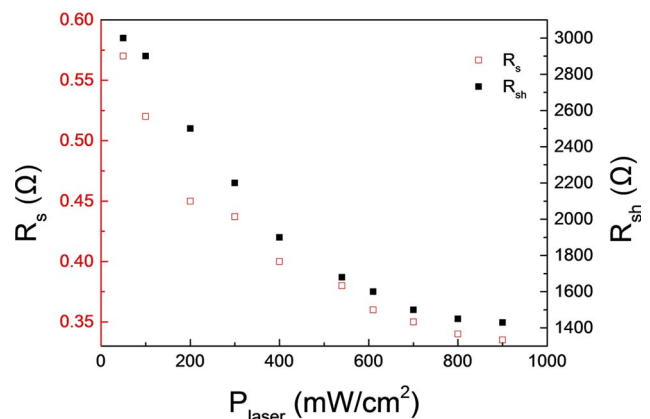


Fig. 6. Effects of P_{laser} on series and parallel resistances.

and body resistance of the cell. With the increase of P_{laser} , the volume resistance decreased as with R_s . However, the contact resistance does not change with the increase of incident energy. When P_{laser} further increased, the influence of bulk resistance on R_s became smaller; consequently, the change rate of R_s decreased^[1].

Figure 7 shows the dependency of n and I_0 on P_{laser} . The trends of the variation of n and $\log(I_0)$ with P_{laser} were analogous to each other. The values of n and I_0 characterized the recombination situation in solar cells. Under low light intensity (as shown when $P_{\text{laser}} < 100 \text{ mW/cm}^2$), carriers recombine through multiple recombination mechanisms, and the recombination rate does not alter with the change of light intensity. Therefore, n and I_0 would not change with the light intensity. With the further increase of light intensity, Auger recombination increases and dominates the recombination in solar cells^[26]. Thus, the values of n and I_0 both increased with increasing P_{laser} , and the rate enlarged gradually.

There was a linear relationship between I_{ph} and P_{laser} , as shown in Fig. 8. Compared with Fig. 3, there was little difference between I_{sc} and I_{ph} .

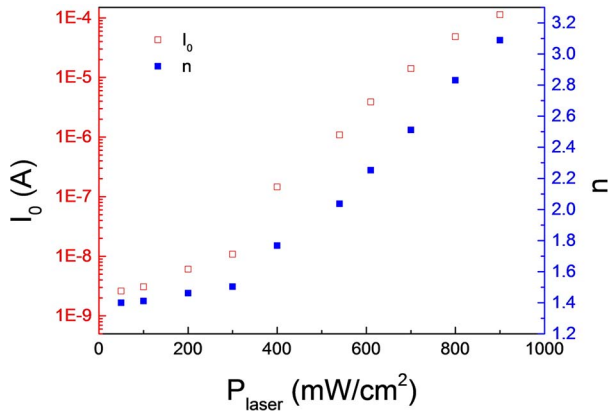


Fig. 7. Effects of P_{laser} on the ideality factor and reverse saturation current.

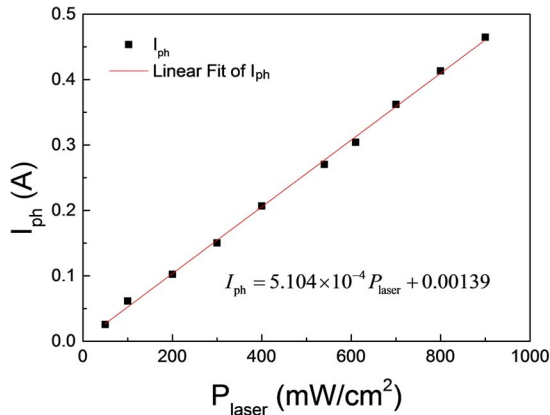


Fig. 8. Effects of P_{laser} on the photo-generated current (the function in the graph is a linear fitting expression)

The quantum efficiency (QE) can be expressed as

$$\text{QE} = \frac{I_{\text{ph}}}{qb_s}, \quad (6)$$

where b_s is the photon flux of the incident light. According to Fig. 8, the total QE of the solar cell irradiated by laser was 0.59. In addition to the internal recombination loss, the reflection loss was more, resulting in lower QE values.

Fill factor is another representation of the curve factor of the I - V curves, which is directly controlled by the series and parallel resistances and ideality factor of the solar cell^[26]. We can conclude from the above discussions that the decrease of shunt resistance and the rise of ideality factor with laser intensity increasing lead to the decrease of the fill factor. The decrease of parallel resistance was also the reason for voltage reduction at the maximum power point. As the QE reflects the utilization of photons, reducing the reflection of the incident laser and the recombination in the cell is an effective way to increase the photo-generated current. Thus, it is a good idea to optimize the structure of solar cells by improving the stability of the parallel resistance under high laser intensity. Moreover, more sophisticated processing technology and fewer defects in solar cells would own a positive effect on the falling of the ideality factor and reverse saturation current. Through the above improvements, the fill factor of the solar cell can be effectively improved, and the conversion efficiency of the solar cell can be enhanced synchronously.

In conclusion, various parameters of $\text{In}_{0.3}\text{Ga}_{0.7}\text{As}$ solar cells under 1070 nm continuous wave (CW) laser irradiation were studied. The parameters of solar cells under different irradiation conditions were extracted by the pollination algorithm. The rationality and accuracy of parameter extraction were verified by comparing the results of calculation and experiment. The experimental results showed that n , I_0 , and I_{ph} increased with increasing P_{laser} , where I_{ph} increased linearly, and n and $\log(I_0)$ had similar evolution trends. R_s and R_{sh} decreased with increasing P_{laser} , and the slope declined. V_m , FF, and η rose at first and decreased subsequently with a similar trend in the range of 50–900 mW/cm^2 . These results show that the performance of solar cells under laser irradiation can be adjusted by selecting the incident laser energy P_{laser} . In addition, reducing the reflection of the solar cell and optimizing the internal recombination can greatly improve the output performance of the solar cell so that it can adapt better in energy transmissions of long distance and high power. Results presented in this Letter can provide a reference in the field of solar cell applications.

This work was supported by the National Defense Basic Scientific Research Program of China (No. JCKY2016606C002), the Shanghai Aerospace Science and Technology Innovation Fund (No. SAST20161113), the National Natural Science Foundation of China

(No. 11774176), and the Fundamental Research Funds for the Central Universities (No. 30918011335).

References

1. P. E. Glaser, *Science* **162**, 857 (1968).
2. T. He, S. Yang, H. Zhang, C. Zhao, P. Xu, J. He, and H. Wang, *Chin. J. Lasers* **40**, 0317001 (2013).
3. Z. Li, Y. Zhang, Y. Ai, and X. Feng, *Laser Technol.* **42**, 306 (2017).
4. Z. Li, D. Shi, J. Shen, and Z. Ma, *Space Electron. Tech.* **3**, 71 (2013).
5. H. Yugami, Y. Kanamori, H. Arashi, M. Niino, A. Moro, K. Eguchi, Y. Okada, and A. Endo, in *IECEC-97 Proceedings of the Thirty-Second Intersociety Energy Conversion Engineering Conference* (1997), p. 625.
6. K. Takeda, M. Tanaka, S. Miura, K. Hashimoto, and N. Kawashima, *Proc. SPIE* **4632**, 223 (2002).
7. N. Kawashima, K. Takeda, and K. Yabe, *Chin. Opt. Lett.* **5**, S109 (2007).
8. J. Mukherjee, S. Jarvis, M. Perren, and S. J. Sweeney, *J. Phys. D Appl. Phys.* **46**, 264006 (2013).
9. C.-W. Wu, J. Wang, and C.-G. Huang, *J. Power Sources* **393**, 211 (2018).
10. F. Khan, S. N. Singh, and M. Husain, *Sol. Energ. Mat. Sol. C.* **94**, 1473 (2010).
11. F. Khan, S.-H. Baek, and J. H. Kim, *Appl. Energ.* **133**, 356 (2014).
12. Priyanka, M. Lal, and S. N. Singh, *Sol. Energ. Mat. Sol. C.* **91**, 137 (2007).
13. V. Lo Brano, A. Orioli, G. Ciulla, and A. Di Gangi, *Sol. Energ. Mat. Sol. C.* **94**, 1358 (2010).
14. D. T. Cotfas, P. A. Cotfas, and S. Kaplanis, *Renew. Sust. Energ. Rev.* **28**, 588 (2013).
15. Y. Li, W. Huang, H. Huang, C. Hewitt, Y. Chen, G. Fang, and D. L. Carroll, *Sol. Energy* **90**, 51 (2013).
16. A. Ortiz-Conde, F. García-Sánchez, J. Muci, and A. Sucre-González, *Facta Universitatis—Series: Electron. Energet.* **27**, 57 (2014).
17. D. F. Alam, D. A. Yousri, and M. B. Eteiba, *Energ. Convers. Manage.* **101**, 410 (2015).
18. O. Mares, M. Paulescu, and V. Badescu, *Energ. Convers. Manage.* **105**, 139 (2015).
19. N. T. Tong and W. Pora, *Appl. Energ.* **176**, 104 (2016).
20. X.-S. Yang, in *Unconventional Computation and Natural Computation: 11th International Conference* (2012), p. 240.
21. Z. Wang, Q. Li, Z. Wang, F. Zou, Y. Bai, S. Feng, and J. Zhou, *Chin. Opt. Lett.* **14**, 081401 (2016).
22. B. Yang, H. Zhang, Q. Ye, H. Pi, C. Shi, R. Tao, X. Wang, and X. Xu, *Chin. Opt. Lett.* **16**, 031407 (2018).
23. R. Mason, "Feasibility of laser power transmission to a high-altitude unmanned aerial vehicle," *Tech. Rep. ADA544926* (Rand, 2011).
24. Shanghai Institute of Space Power-Sources, *Physics Power Technology* (Science Press, 2015).
25. M. Wolf and H. Rauschenbach, *Adv. Energy. Conver.* **3**, 455 (1963).
26. J. Nelson, *The Physics of Solar Cells* (Shanghai Jiao Tong University, 2011).
27. O. Breitenstein, J. P. Rakotoniaina, M. H. Al Rifai, and M. Werner, *Prog. Photovoltaics* **12**, 529 (2004).